crystals

MDPI

Article

The Structural Characteristics and Chemical Composition of Serpentine Jade Weathering Rinds: Implications for the Formation Process

Shanna Xue [1], Mingyue He [1,*], Mei Yang [2,*] and Shaokun Wu [1]

[1] School of Gemmology, China University of Geosciences, Beijing 100083, China
[2] Sciences Institute, China University of Geosciences, Beijing 100083, China
* Correspondence: hemy@cugb.edu.cn (M.H.); yangmei@cugb.edu.cn (M.Y.)

Abstract: Weathering rind retains the greatest extent of the mineralogical and chemical composition information of the original mineral. Recently, we found some brownish-yellow or khaki serpentine jade weathering rinds with a thickness of 0.2–0.6 cm in Ji'an. The purpose of this paper is to explore differences in structural characteristics and chemical composition between weathering rinds and unweathered cores and summarize the formation of weathering rinds. In terms of structural characteristics, weathering rinds have smaller a_0, b_0, β values than unweathered cores; the specific surface area is 13.3987 m^2/g; the pore volume is 0.0314 cm^3/g; and the pore size distribution is characterized as more mesoporous (2–10 nm). The weathering rind shows partial dissolution of serpentine grains, increased porosity, and loosening structure. In terms of chemical composition, the weathering rind is characterized by the decrease of some serpentine major elements (Si, Mg, and Fe) and the increase of some impurity elements (Al, Ca, K, Na, and Cl). The weathering rind is the result of further alteration of serpentine jade, accompanied by the reduction of the Fe^{3+}/Fe^{2+} ratio and the generation of the clay mineral (chlorite). In addition, it was also found that Ji'an serpentine jade belongs to Mg-bearing carbonate rock genesis, which are derived from marine deposits.

Keywords: weathering rinds; structural characteristic; chemical composition; formation process; Mg-bearing carbonate rock

Citation: Xue, S.; He, M.; Yang, M.; Wu, S. The Structural Characteristics and Chemical Composition of Serpentine Jade Weathering Rinds: Implications for the Formation Process. *Crystals* **2023**, *13*, 239. https://doi.org/10.3390/cryst13020239

Academic Editor: Vladislav V. Gurzhiy

Received: 11 December 2022
Revised: 27 January 2023
Accepted: 28 January 2023
Published: 30 January 2023

1. Introduction

Ji'an Serpentine Jade, also known as "Anlv jade", is located in the Liao-Ji rift zone in the southern Jilin Province [1,2]. The study of Ji'an serpentine jade has been relatively detailed; its predecessors were examined from a range of perspectives, including genesis [3–5], spectral characteristics [6–8], and mineralogical properties [9–11]. However, the study of serpentine jade weathering rinds is largely lacking. Weathering rinds are alteration zones where the original mineral has been modified and/or the chemical composition has undergone some alteration, usually followed by oxidation and secondary precipitation [12–15]. Most of the samples studied for weathering rinds are rocks, and Oguchi (2001) summarized the rock types studied so far, e.g., andesite, basalt, granite, sandstone, granodiorite, gneiss, and quartz porphyry (see Table 1 of [15]). In addition, there are some studies of nephrite weathering rinds [14,16]. Grapes (2010) analyzed the geochemistry of a New Zealand nephrite weathering rind and suggested that higher porosity created by actinolite dissolution results in an exponential increase in the amount of weathering (consistent with dissolution and secondary precipitation).

The study of weathering rinds mainly focuses on two key themes. On the one hand, it analyzes the mineralogical, chemical, mechanical, and colorimetric properties of weathering rinds [12,14,17–19]. On the other hand, the thickness of the weathering rind is used as an indicator of the relative ages of glacial and periglacial deposits in high mountain areas [12]. The study of the structural characteristics of weathering rinds is of great significance,

which can also be analyzed by the pore size distribution characteristics of weathering rinds. The microscopic morphology of pores can be obtained by continuous imaging of SEM images [20–22]. Liu (2018) used SEM to observe the morphological characteristics of the surface pores of turquoise and calculated the surface porosity of turquoise at different densities treated by dipping or sealing wax [23]. In recent years, the BET method has also been widely used [24–27]. This method can quantitatively analyze the pore characteristics of samples and has certain applications in the study of gemstones. Li et al. (2016) used the BET method to analyze the pore distribution characteristics of natural turquoise and electrochemically treated turquoise and identified structural differences between the two.

Table 1. The relative densities of weathering rinds and unweathered cores.

Samples	W.r-1	W.r-2	W.r-3	U.r-1	U.r-2	U.r-3	Serpentine
relative density (g/cm^3)	2.417	2.354	2.388	2.455	2.491	2.502	2.57(+0.23, −0.13)

W.r, weathering rind; U.r, unweathered core.

In addition, the genesis and formation process of weathering rinds have always been the focus of research, and most scholars hold their own views, e.g., dissolution only [13], both oxidation and dissolution [14,15,18,19], loss of mobile elements and concentration of immobile elements [14,28], and local climate environment and biochemical processes [29,30], particularly the formation of iron-rich rock coatings, can be explained [13,17,31].

Here, we found some serpentine jades with weathering rinds of different thicknesses in Ji'an, Jilin Province, and analyzed them by structural observation (SEM), XRD, BET test, μ-XRF mapping, and major and trace element testing. The purpose is to analyze the difference of structural characteristics and chemical composition between weathering rinds and unweathered cores, summarize the formation process and genesis of weathering rinds in this area, and further improve the geological characteristics of Ji'an serpentine jade weathering rinds.

2. Materials and Methods

The serpentine jade samples used in this study were collected along the green river near Ji'an, Jilin Province, China. We selected four representative samples (GT-09, GT-07, GT-20, and GT-21) from dozens of samples for this study (Figure 1). Most of the samples have a layer of weathering rind ranging in size from 0.2 to 0.6 cm, and the color changes from yellowish green to light yellow to brown yellow or khaki (Figure 1a). Weathering rind is defined for the purposes of this study as a band of alteration whose inner band approximately parallels the outer surface of serpentine jade by the weathering effect [12].

Figure 1. Sample photographs. (**a**,**b**) Serpentine jade samples collected from Gaotai area, Ji'an Province; (**c**,**d**) Serpentine jade samples with weathering rind after crushing.

Weathering of rinds is layered, but vague, diffuse inner parts of rinds known as inner bands were not measured (Figure 1c) because they are difficult to extract. Moreover, it is impossible to analyze its weathering process and genesis separately from the outer brown yellow band. However, many studies have shown that the causes of inner bands and outer weathering bands are in a transitional relationship. Some cracks on the weathering rind were observed under hand specimens and a microscope; a large number of black metal minerals (magnetite) and pale-yellow carbonate veins (dolomite) invaded the interior of jade from the weathering rind cracks, and secondary minerals such as dolomite, magnetite, chlorite, and humite (Figure 1d) also were observed.

The structure of weathering rinds and unweathered cores was observed by using a SUPRA 55 scanning electron microscope (SEM) under 20 kV at the China University of Geosciences (Beijing). The gas adsorption method was tested by a Micromeritics ASAP 2460 specific surface area and pore size analyzer produced in the United States. The adsorbed gas is N_2, the degassing temperature is 200 °C, and the degassing time is 12 h. The 0.3–0.4 g weathering rinds and unweathered cores were crushed into powder for examination after being vacuum dried for 24 h.

The X-ray diffraction (XRD) experiment was tested by the SmartLab (9 KW) X-ray powder diffractometer that was equipped with a conventional copper target X-ray tube (set to 40 kV and 200 mA) and a graphite monochromator at the Institute of Earth Science, CUGB. In the continuous scanning mode, a step length is 0.02° in the range of 3–90° is taken at a scanning speed of 4 °/min. The samples were made into 200 mesh powders and stored immediately to minimize contamination and oxidation. The results were normalized and analyzed using the MDI Jade 6.5 software.

The distribution mapping of elements in a sample thin section was measured by μ-XRF spectroscopy at CUGB. The system worked at 50 kV and 300 μA, and the spot size was 20 μm. The major elements of weathering rinds and unweathered cores on the polished thin section were obtained by an EPMA-1720 electron microprobe at the Electron Probe Laboratory, CUGB. The primary analyzing settings were a 1μm beam spot diameter, a 10 nA beam, and a 15 kV acceleration voltage.

At the Mineral Laser Microprobe Analysis Laboratory (Milma Lab) in the Institute of Earth Science, CUGB, the trace element data was analyzed by using Laser Ablation-Inductively Coupled Plasma Mass Spectrometry (LA-ICP-MS), which is equipped with a RESOLution S155 LR 193 nm ArF excimer laser ablation system and an Agilent 7900 quadrupole ICPMS. The laser repetition rate of 5 Hz at 3 J/cm^3 and a spot size of 33 μm were used in this analysis. NIST 610 and BCR-2G were used as the external standards, and the internal standard was taken from EPMA result data.

3. Results

3.1. Microstructure Characteristics

Serpentine's interference color is primarily grayish-white. The interference color of serpentine at the weathering rind is primarily yellowish-white (Figure 2a,b), and sometimes an abnormal interference color is noticed that is different from the grayish-white of the unweathered cores. According to research done using optical microscopy, the level of serpentine crystallization varies between the weathering rind and the unweathered core. The serpentine in the unweathered core has better morphology and is mainly euhedral, whereas the serpentine in the weathering rind is generally xenomorphic and hypautomorphic of serpentine crystals, the aggregate is primarily flaky or fibrous, and the serpentine crystals have partial dissolution at the edge (Figure 2e,f). In addition, a few carbonate veins can be found at the weathering rind that extend from the cracks into the core of the jade (Figure 2d), reflecting the serpentine jade's original rock type (Mg-bearing carbonate rock) in Ji'an. The structure of serpentinite mainly includes microscopic scaly structure, blade-like structure, and replacement remnant structure (Figure 2c). The unweathered core is primarily characterized by replacement remnant structure and lamellar stacking

structure, but the weathering rind in this study is characterized by fibrous interwoven structure, with a relatively loose structure and significantly increased porosity (Figure 2h).

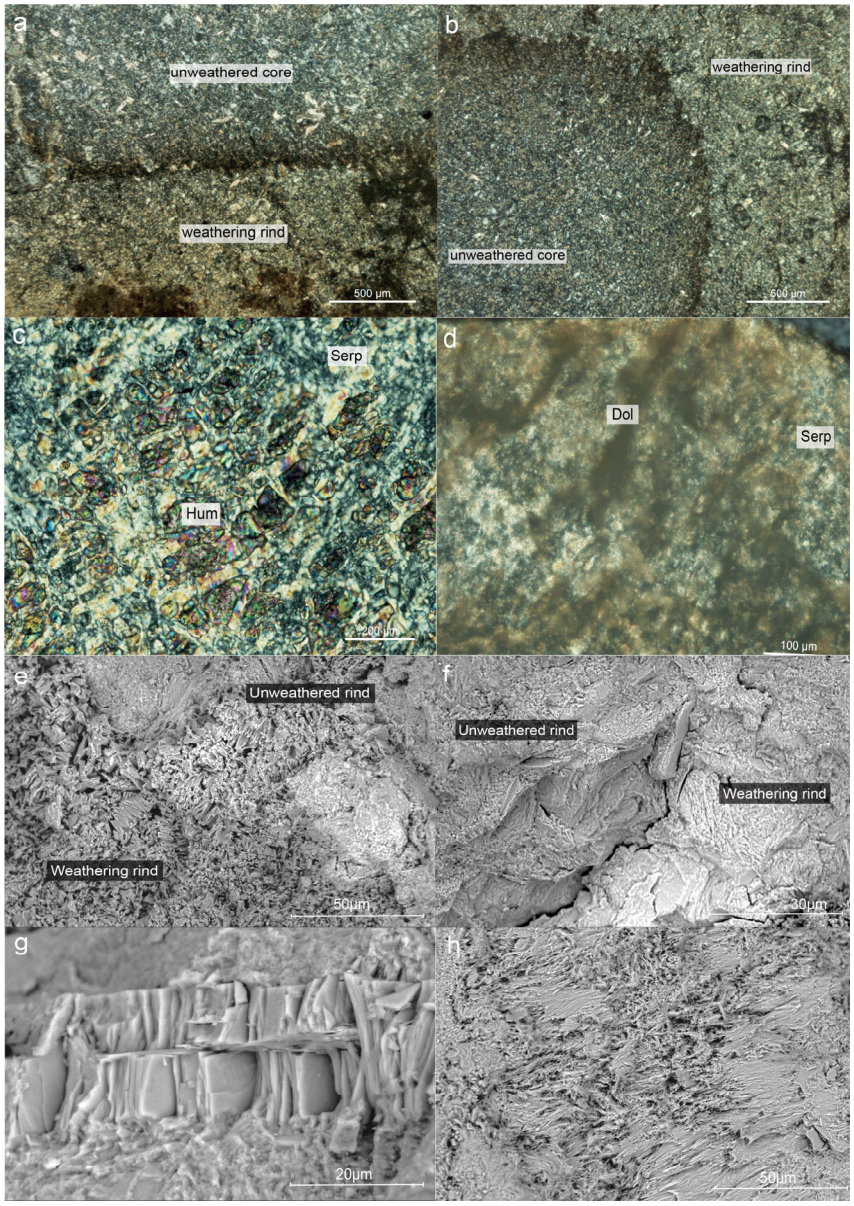

Figure 2. Microstructure characteristics of weathering rinds and unweathered cores observed under CPL and SEM. (**a**,**b**) The overall feature of weathering rinds and unweathered cores under CPI; (**c**) The replacement remnant structure of unweathered cores; (**d**) Several carbonate veins intrude into the interior of the jade from the weathering rind; (**e**,**f**) The overall feature of weathering rinds and unweathered cores under SEM; (**g**) The flaky stacking structure of unweathered cores; (**h**) The fibrous interwoven structure of weathering rinds.

The sample for the relative density test should be separated from the serpentine jade in advance. During the test, it was discovered that samples of weathering rind showed evident bubbling throughout the test, indicating that the structure of weathering rinds is loose. The water squeezed out the gas in the void, causing the test results to have some errors; thus, it is important to immediately read the figure when it is stable. In addition, in order to further limit experimental error, the sample should be thoroughly dried out in the oven before being tested again. The relative densities of the weathering rinds of the samples (Table 1) ranged from 2.39 to 2.42, while the standard value of the serpentine jade is 2.57 (+0.23, −0.13). In addition, all mineral composition-related test results in this study

indicate that the majority of the serpentine jade from Ji'an is still primarily composed of serpentine, so the much smaller relative density values than serpentine reflect the loose structure of the weathering rind.

3.2. Nitrogen Adsorption by the BET Method

From the SEM and relative density test, it can be seen that the serpentine crystal of the weathering rind has partial dissolution, increased porosity, and loose structure (Figure 2), which is speculated to be caused by weathering. Further quantitative analysis of the weathering rind and unweathered core was carried out by the gas adsorption method. The specific surface area of the weathering rind was calculated to be 13.3987 m^2/g by the BET equation [32] derived by Brunauer, Emmett, and Teller, which was much larger than that of the unweathered core (8.8020 m^2/g). The pore volumes were calculated by the BJH method [32–34] to be 0.0314 cm^3/g and 0.0167 cm^3/g, respectively. Figure 3a is the adsorption isotherm of the weathering rind. According to the six types of standard adsorption isotherms made by IUPAC, it can be seen that the adsorption isotherm of the weathering rind belongs to the IV isotherm type. The typical characteristic of this kind of isotherm is that the adsorption branch is inconsistent with the desorption, and there is an obvious hysteresis phenomenon, which is usually caused by mesopores in the material structure [35]. In addition, Figure 3b shows the pore size distribution of the weathering rind and unweathered core. The figure indicates that both of them are more mesoporous pores (2–10 nm), with a small number of micropores (0–2 nm) and no large pores (>50 nm). In addition, it can be found that the pore size of the weathering rind is much larger than that of the unweathered core.

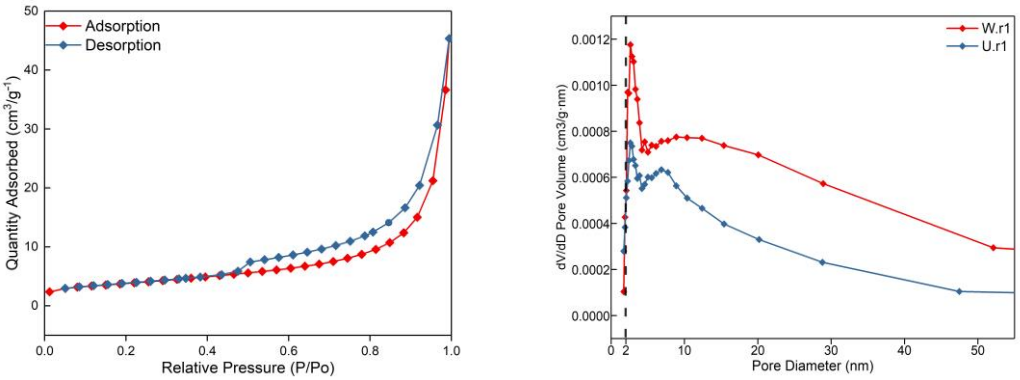

(**a**) (**b**)

Figure 3. Figures of nitrogen adsorption for the weathering rind and unweathered rind: (**a**) Adsorption-desorption isotherms in the weathering rind; (**b**) Adsorption-desorption isotherms in the weathering rind and the unweathered rind.

3.3. X-ray Diffraction

The XRD patterns of weathering rinds and unweathered cores with standard XRD patterns are shown in Figure 4. Both have patterns identical to that of lizardite-1T (PDF 86-0403), with strong peaks at d(001) = 12.079–12.132° and d(002) = 24.301–24.403° and medium intensity peaks at and d(−131) = 36.007°, which indicates that the major mineral of Ji'an serpentine jade is lizardite, which is consistent with previous studies [7]. In addition, unlike the unweathered core, the weathering rind was observed to also show characteristic chrysotile peaks and chlorite peaks, which suggested that the weathering rind was further serpentinizing and that clay minerals were created during weathering. Weathering rinds have a pattern identical to that of chrysotile (PDF 27-1275), showing strong peaks at d(002) = 12.031° and d(004) = 24.299°, and medium intensity peaks at d(131) = 34.300° and d(060) = 60.153°. In addition, several peaks for weathering rinds XRD patterns can be found, which are matched with chlorite (PDF 07-0078), with strong peaks at d(002) = 6.263° and d(002) = 12.510° and medium intensity peaks at d(004) = 25.128°and d(131) = 34.798°.

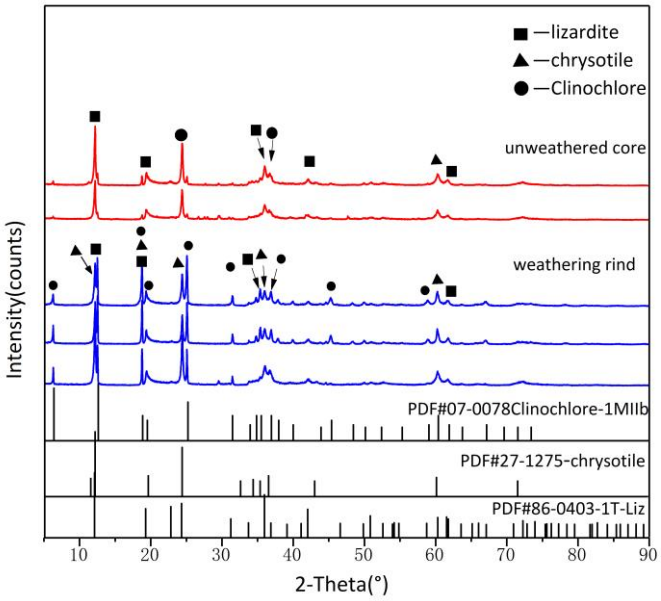

Figure 4. The XRD patterns of weathering rinds and unweathered cores.

The lattice parameters result from the comparison of the collected data with the standard data for lizardite, and both are summarized in Table 2 below. The lizardite is a monoclinic system, with a_0 = 0.531 nm, b_0 = 0.920 nm, c_0 = 0.731 nm, β = 90°. As can be seen from Table 2, the a_0, b_0, and β of the weathering rind lattice parameters are much less than those of the serpentine jade that has not weathered, and both are closer to the standard values of the lizardite. Combined with the chemical formula of serpentine, it is not difficult to see that the values of a_0, b_0, and β increase with the increase of Fe^{3+} substituted Mg^{2+} in octahedral sheets, while the value of c decreases with the increase of Fe^{3+} replaced Mg^{2+}, and the value of a_0, b_0 also decrease when there are vacancies in octahedral sheets. It can be inferred that the Fe^{3+} in weathering rinds is much smaller than that in unweathered cores. In addition, the lattice parameters of minerals are influenced by the water concentration in the interlayer.

Table 2. Lattice parameters of weathering rinds and unweathered cores.

Lattice Parameters	Weathering Rinds	Unweathered Cores	Lizardite
a_0/nm	0.529	0.531	0.531
b_0/nm	0.924	0.926	0.920
c_0/nm	0.731	0.731	0.731
β (°)	89.586	89.908	90

The lattice parameters of samples in the table are average values.

3.4. μ-XRF Mapping

To intuitively observe the chemical composition difference in different areas, μ-XRF mappings were performed on a thin section with the weathering rind and unweathered core, and the results are shown in Figure 5. It is noticed that the relative increase in Ca and Al content from the unweathered core to the weathering rind and the relative decrease in Si, Mg, and Fe content. The element change reveals the decrease of major elements in serpentine (Si, Mg) and the increase of impurity elements (Al, Ca, Fe, Ti).

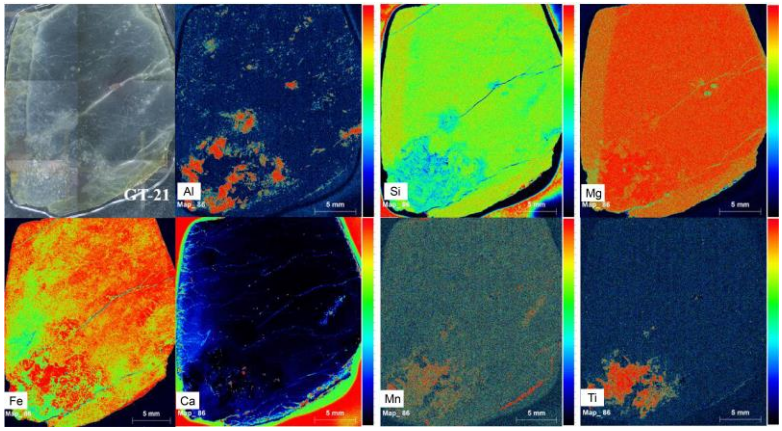

Figure 5. Elemental distribution maps made by μ-XRF mapping on a thin section with a weathering rind and an unweathered core.

3.5. EPMA

The chemical formula of serpentine is $Mg_6[Si_4O_{10}](OH)_8$. Previous studies have shown that the genesis of serpentine jade in Jilin is due to the type of Mg-bearing carbonate rock and that the content of Mg is relatively high. The EPMA shows that the content of Mg in both areas is high (Table 3), which is combined with the previous μ-XRF mapping results. Figure 6 shows the change of the content of major elements in both, suggesting that the content of SiO_2, MgO, H_2O, Fe_2O_3, and FeO is negatively correlated with the thickness changes from the weathering rind to the unweathered core and that the content of Al_2O_3, CaO, and H_2O showed a positive correlation.

Table 3. The EPMA data of the weathering rind and unweathered core samples (wt%).

Date	W.r-1	W.r-2	W.r-3	U.r-1	U.r-2
SiO_2	33.03	32.71	39.97	44.03	42.4
TiO_2	0.04	0	0	0.07	0
MgO_2	36.92	35.93	37.33	45.51	43.33
K_2O	0.02	0.02	0.02	0.06	0.02
Cr_2O_3	0.02	0.07	0	0.02	0
Al_2O_3	17.10	18.42	9.31	0.13	0.29
CaO	0.06	0.01	0.03	0.06	0.01
MnO	0	0	0.05	0.06	0.03
FeO *	0.89	0.86	0.53	1.32	1.53
Fe_2O_3 *	0	0	0	0.18	0.48
NiO	0.05	0.04	0.02	0	0
Na_2O	0.04	0.05	0.08	0.02	0.01
# H_20	1.79	1.71	2.6	1.48	1.9
Total	88.21	88.29	87.40	88.52	88.1

W.r, Weathering rind. U.r, Unweathered core. *, Calculated FeO and Fe_2O_3. #, Calculated H_2O.

According to the results of major elements, it can be seen that major elements such as Si, Mg, Fe^{2+}, and Fe^{3+} in the weathering rind decrease, while the contents of Ca and Al increase. In addition, it is discovered that the amount of H_2O in the weathering rind increases, and it is preliminarily speculated that the decreases of Fe^{3+} content, the replacement of Mg^{2+} in the octahedral sheet, or the larger Si^{4+} in the tetrahedral sheet, as well as the decrease of some major elements, led to an increase in the porosity and caused H_2O to concentrate at the weathering rind.

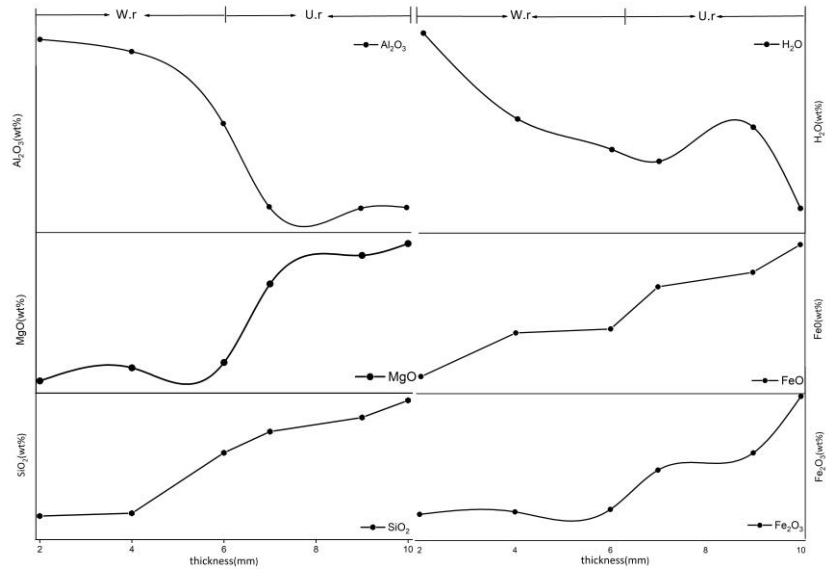

Figure 6. Changes in chemical composition of weathering rinds and unweathered cores with different thicknesses.

3.6. LA-ICP-MS

The results of trace element analysis (Table 4) show that the overall trace elements of serpentinite jade from Ji'an are relatively low and are generally enriched in LILE such as K, Rb, Th, and U and deficient in HFSE such as Nb, Sr, and Ti; the total rare earth elements (ΣREE) of the six samples ranged from 0.28 to 0.55 ppm. Weathering rinds are enriched in K, Na, Ca, and S elements compared to unweathered cores, indicating that the formation of the weathering rind is related to the increase of impurity elements. Trace element concentrations normalized to chondrite of samples (Figure 7) suggest that the overall pattern of high left and low right indicates that the LREE are more enriched than the HREE, and the ratio of light to heavy rare earth elements (LREE/HREE) is large (4.50–5.00), in which the inclination of the LREE section is large and the divergence is obvious, and the HREE section is gentle, with slight negative anomalies of Eu and Ce (δEu = 0.95–1.47; δCe = 0.78–0.98).

Table 4. The trace elements of the weathering rind and the unweathered serpentine jade (ppm).

Date	W.r-1	W.r-2	W.r-3	U.r-1	U.r-2	U.r-3
Li	0.069	0.076	0.097	0.010	0.010	0.024
B	19.9	15.2	12.1	24.07	14.23	15
Ti	27.9	59	3.43	2.56	1.38	1.95
K	50	60.5	60	0.72	1.019	560
Na	1280	1560	1660	4.33	3.85	320
Ca	720	940	900	6.4	5.2	320
V	0.41	0.7	0.06	0.026	0.044	0.043
Cr	0.49	2.47	0.14	0.128	0.121	0.125
Co	0.148	0.331	0.056	0.168	0.23	0.065
Ni	0.31	0.24	0.153	0.253	0.268	0.221
Sr	0.626	0.91	0.718	0.057	0.032	0.275
Zr	0.56	0.67	0.67	0.058	0.066	0.27
Cl	43	71	44	23.3	21.8	27.8

Table 4. *Cont.*

Date	W.r-1	W.r-2	W.r-3	U.r-1	U.r-2	U.r-3
S	62	66	41.6	27.7	26.9	30.7
La	0.141	0.148	0.086	0.081	0.067	0.077
Ce	0.183	0.234	0..156	0.112	0.094	0.135
Pr	0.015	0.016	0.014	0.01	0.008	0.012
Nd	0.055	0.064	0.049	0.03	0.027	0.051
Sm	0.01	0.008	0.006	0.003	0.004	0.009
Eu	0.002	0.002	0.001	0.002	0.002	0.002
Gd	0.007	0.009	0.005	0.004	0.005	0.002
Tb	0.001	0.002	0.001	b.d.l	b.d.l	0.001
Dy	0.007	0.001	0.007	0.004	0.003	0.007
Ho	0.001	0.006	0.001	0.001	0.001	0.001
Er	0.007	b.d.l	0.006	0.003	b.d.l	0.004
Tm	0.001	0.011	0.001	0.001	0.001	0.001
Yb	0.012	0.002	0.006	0.007	0.01	0.006
Lu	0.005	0.049	0.001	0.002	0.002	0.002
Y	0.045	0.558	0.042	0.029	0.021	0.034
Th	0.038	0.044	0.053	0.004	0.005	0.019
U	0.014	0.018	0.015	0.005	0.005	0.014

W.r, weathering rind. U.r, unweathered core; b.d.l., below the detected line.

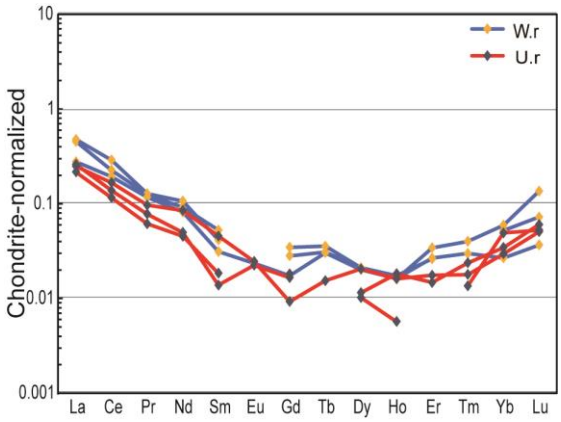

Figure 7. Chondrite normalized trace element spider diagrams for samples [36].

4. Discussion

4.1. The Structure Characteristics of Weathering Rinds and Unweathered Cores

The specific surface area, pore volume, and average pore size of the weathering rind are much larger than those of the unweathered core. The larger the value, the higher the possibility that the weathering rind is stored by gas adsorption, resulting in a loose structure and increased porosity. The distribution of pore volume shows that the weathering rind has more mesopores, accounting for 80%, indicating that the micropores and mesopores (2–10 nm) in the weathering rind provide the main specific surface area and pore volume, which is also the main place for gas adsorption and storage [27]. Combined with SEM observation, it was found that the serpentine crystals in the weathering rind were fibrous and disorderly arranged. Some dissolution occurred at the edges of the crystals, and there was also a large gap between the grains. Due to weathering at the weathering rind, the original slender serpentine crystals were divided into many slender needle-like

serpentine crystals, showing the structural characteristics of chrysotile. The closer to the external serpentine crystal, the smaller the size and the higher the porosity, indicating that the structure of the serpentine becomes very loose after weathering and the porosity increases significantly. In addition, according to the four types of hysteresis loops made by their predecessors, the IV adsorption isotherm of the weathering rind belongs to the H3 hysteresis loop. This hysteresis loop type is formed by flake granular materials (such as clay minerals) or materials with narrow gaps, which have larger voids and wider pore sizes [34]. Therefore, it can be seen that the emergence of the H3 type hysteresis loop indicates the possibility of clay mineral generation at the weathering rind.

4.2. The Formation Mechanism of Weathering Rinds

The formation of weathering rinds involves both physical and chemical components [15,18,19]. Both XRD and major and trace tests have revealed the presence of chrysotile and clay minerals (chlorite) in weathering rinds, chrysotile being a further alteration mineral based on lizardite that forms at temperatures above 200 °C [37]. On the other hand, chlorite proves the presence of clay minerals in the weathering rind, indicating that serpentine is weakly resistant to weathering. The formation process of most weathering rinds is accompanied by the generation of clay minerals, and the better-developed clay minerals are at least partly due to the weathering of original minerals [28]. Chlorite forms in alkaline, weakly leaching environments and is usually enriched in high-latitude continental soils and sediments, and most previous studies have shown that the presence of chlorite and illit is a sign of weak weathering intensity [38,39].

In terms of structural characteristics, the weathering rind has a loose structure and increased porosity; in terms of chemical composition, the weathering rind has increased impurity elements such as Al, Ca, K, Cl, and Na and decreased major elements of serpentine such as Mg, Si, and Fe (Figure 6). Most of the studies suggested that the oxidation of Fe existed in the weathering rind [12,14,15,37]. However, the Fe^{2+} and Fe^{3+} of the weathering rind that we observed were lower than those of the unweathered core, which was inconsistent with the previous findings. Here we suggest that the reduction of Fe is related to the fact that this element is a coloring element of serpentine jade. The key factors influencing the color of serpentine jade in Ji'an are the Fe^{2+}-Fe^{3+} charge transfer and the d-d electron transition of Fe^{3+} ions [40,41]. The absorption of the Fe^{3+} d-d electron transition diminishes until it disappears when Fe^{3+}/Fe^{2+} is smaller than 1, causing the color to appear green. The lack of Fe^{3+} content, the reduction of the Fe^{3+}/Fe^{2+} ratio, and the increase in impure elements can be seen in the transition from the yellowish green of unweathered cores to the brownish-yellow and even khaki of weathering rinds. In addition, the decrease in Fe content is also related to the dissolution of serpentine grains and the outflow of minerals into the river.

Ji'an serpentine's protolith is Mg-bearing carbonate rock, and its metallogenic environment is medium-low temperature hydrothermal alteration. According to Table 4, there is a certain amount of the Cl element (23.3–27.8 ppm) in the unweathered serpentine, suggesting the participation of salt ions in low temperature hydrothermal solutions. Due to the low Cl content, which is lower than the general value of seawater salinity, it is speculated that the addition of non-magma fluid and fluid boiling will lead to a decrease in the Cl content [42]. In the weathering rind, the Cl content is twice as high as that of the unweathered serpentine (43–71 ppm). It is speculated that the influence of the nearby river water and groundwater (which contain quite high Cl and F) during weathering leaches so that the Cl content in the weathering rind is relatively increased. Because only the data on Cl content is not enough to support more conclusions, further evidence (such as the source of ore-forming fluid) needs to be obtained by fluid inclusion test analysis.

Based on the results of petrographic and chemical composition analysis and combined with previous studies, we summarize the formation process of weathering rinds of serpentine jade in Ji'an. In general, the weathering rind of Ji'an serpentine jade is the weathering band of further alteration of serpentine, the formation process is accompanied by the gener-

ation of clay minerals and secondary precipitation of serpentine crystals, and the degree of weathering is weaker than that in lower latitudes because it is in a high latitude area [28]. The specific formation process can be demonstrated as the unweathered serpentine jade was exposed to the ground for a long time; the weathering effect caused the serpentine grain outside the jade to dissolve and the porosity to increase. In addition the long time in the river resulting in a near erosion effect in the flowing water with displacement of H_2O into the pores, and removal of external impurities, resulting in the reduction of some major elements and the gathering of some impure elements, dissolving of serpentine grains, change in color, loosening of the structure, and decrease in density. In this process, the color of serpentine jade gradually changes from yellow-green to an inner light-yellow rind and then develops a brownish yellow or even khaki weathering rind because the decrease in Fe^{2+} and Fe^{3+} content and the Fe^{3+}/Fe^{2+} ratio are correlated with the color change of both.

4.3. The Genesis Analysis of Serpentine Jade in Ji'an

The major and trace elements can reveal information about the genesis type, protolithic characteristics, and sedimentary environment of serpentine jade. The serpentine jade in Ji'an is found in the serpentinized marble in the MayiHe Formation of the Ji'an Group, which is located in the Liao-Ji Proterozoic rift zone [1]. Trace elements have a certain indicative significance for the genesis of serpentine jade. Cr, Co, and Ni are typical compatible elements, mainly enriched in mantle-derived or mantle-related rock systems. Among them, Cr and Ni are strongly compatible elements with different geochemical properties. Cr and Al form isomorphic substitutions, mainly in spinel and clinopyroxene. In olivine, Ni and Mg form an isomorphous substitution [43,44]. Dong et al. (2016) found that the amounts of Cr, Co, and Ni in Mg-bearing carbonate rocks are significantly lower than those in ultrabasic rocks after analyzing the trace elements of serpentine jades from two different origins. The 3D scatter plot of the Cr, Co, and Ni contents of serpentine jade from Ji'an and other places [43,45,46] is shown in Figure 8. It can be seen that the Cr, Co, and Ni content of serpentine jade in Ji'an is similar to that of serpentine jade of Mg-bearing carbonate origin, so we can infer that its genetic type is Mg-bearing carbonate rock.

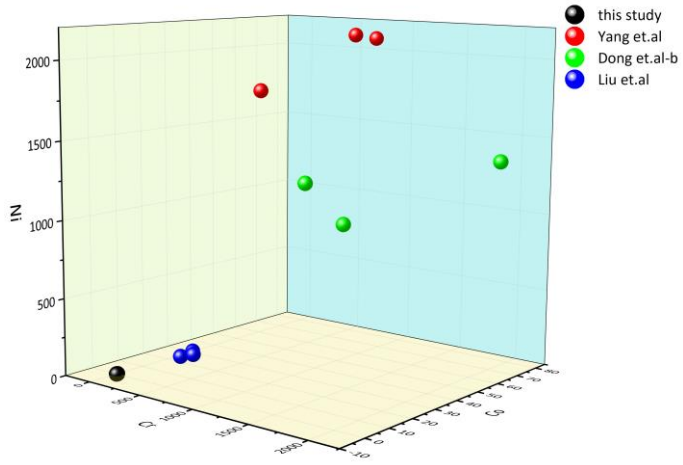

Figure 8. The 3D scatter plot of Cr, Co, and Ni elements [43,45,46].

Between sedimentary carbonate rocks and magmatogene carbonatites, there are significant changes in their geochemical properties. Taylor and McLennan (1985) proposed that sedimentary carbonate rocks are rich in U and poor in Th, and the contents of trace elements such as Zr and Nd are lower than the average content in the crust, while magmatogene carbonatites are just the opposite [47,48]. The w(Th)/w(U) values of the samples in this study range from 0.91 to 2.73. According to the ratio of Th to U and trace elements such as Nd and Zr, it is reasonably inferred that the protolith of serpentine jade in this study area is sedimentary carbonate rock. Ce content would become comparatively deficient under the effect of sediment, reflecting that its original rock formation was exposed to biological

or chemical deposition during the marine phase and that the depositional environment was generally constant. In addition, major elements can also determine the sedimentary environment of the stratum. The value of W(Al)/W(Al + Fe + Mn) in sedimentary rocks can be used to identify the source of sedimentary materials. When the value is greater than 0.5, the source should be a land source, and when the value is less than 0.5, it is hot water deposition [49]. The W(Al)/W(Al + Fe + Mn) values of the studied samples range from 0.17–0.25, indicating that the sediment source of the serpentinized marble in Ji'an may be from marine sedimentation with hot water deposition during the formation process.

5. Conclusions

(1) The density of the weathering rind of Jilin Ji'an serpentine jade is 2.36–2.42 g/cm^3, which is lower than the standard value of serpentine. The specific surface area is 13.3987 m^2/g and the pore volume is 0.0314 cm^3/g, which is much larger than the unweathered jade. Both are characterized by mesoporous (2–10 nm) distribution, accounting for about 80%. The adsorption isotherm of the weathering rind belongs to the IV isotherm type, H3 hysteresis type, and the structural characteristics show that serpentine crystals appear partially dissolved in the weathering rind, with increased porosity and a loose structure.

(2) The major trace element test shows that Ji'an serpentinite belongs to the Mg-bearing carbonate rock genesis, which is marine sedimentation with a relatively stable depositional environment. Overall, the serpentine jade is enriched in LILE such as K, Rb, Th, and U, and deficient in HFSE such as Nb, Sr, and Ti. ΣREE is 9.55–12.99 ppm, and Eu and Ce elements are slightly negative anomalies after chondrite-normalized.

(3) Ji'an serpentine jade weathering rind is the weathering band with further alteration of serpentine, accompanied by the dissolution of serpentine grains and the reduction of the Fe^{3+}/Fe^{2+} ratio in the process. It can be explained as follows: weathering increases the porosity of the exterior of serpentine jade, and long-term exposure to water erosion near rivers causes H_2O and external impurities to enter pores. This causes the decrease in some major elements (Si, Mg, and Fe) of serpentine and the concentration of impurity elements (K, Na, Ca, Al, and Cl), the dissolution of serpentine grains, the generation of clay mineral (chlorite), structural loosening, the change in color, and finally the formation of a brownish-yellow or khaki weathering rind.

Author Contributions: Conceptualization, M.H.; methodology, M.H. and M.Y.; software, S.X. and S.W.; formal analysis, S.X. and S.W.; investigation, S.X. and S.W.; data curation, S.X.; writing—original draft preparation, S.X. and S.W.; writing—review and editing, S.X. and M.Y.; supervision, M.H. and M.Y.; funding acquisition, M.H. All authors have read and agreed to the published version of the manuscript.

Funding: National Mineral Rock and Fossil Specimens Resource Center.

Institutional Review Board Statement: Not applicable.

Informed Consent Statement: Not applicable.

Data Availability Statement: Not applicable.

Acknowledgments: We thank the laboratory of the National Mineral Rock and Fossil Specimens Resource Center for experimental help.

Conflicts of Interest: The authors declare no conflict of interest.

References

1. Qin, Y. Geochrnoligicl Constraints on the Tectonic Evolution of the Liao-Ji Paleoproterozoic Rift Zone. Ph.D. Thesis, Jilin University, Changchun, China, 2013.
2. Wang, Y.; He, M.; Yan, W.; Yang, M.; Liu, X. Jianite: Massive Dunite Solely Made of Virtually Pure Forsterite from Ji'an County, Jilin Province, Northeast China. *Minerals* **2020**, *10*, 220. [CrossRef]

3. Chen, Q.; Wang, Y.Y.; Gan, F.X. The Chemical Compositions and Origin Characters of Serpentine Jade from Different Deposits. *Appl. Mech. Mater.* **2014**, *624*, 119–123. [CrossRef]
4. Wang, Y.Y.; Gan, F.X.; Zhao, H.X. Inclusions of Black-Green Serpentine Jade Determined by Raman Spectroscopy. *Vib. Spectrosc.* **2013**, *66*, 19–23. [CrossRef]
5. Zhang, B.S.; Wu, X.T.; Sun, Y.F.; Ritchey, M.; Fan, A.C.; Zhang, Y.Y.; Yu, G.; Song, Y.B. Complex Raw Materials and the Supply System: Mineralogical and Geochemical Study of the Jade Artefacts of the Longshan Culture (2400–2000 Bce) from Sujiacun Site in Coastal Shandong, China. *Archaeometry* **2021**, *63*, 1–18. [CrossRef]
6. Kloprogge, J.T.; Frost, R.L.; Rintoul, L. Single Crystal Raman Microscopic Study of the Asbestos Mineral Chrysotile. *Phys. Chem. Chem. Phys.* **1999**, *1*, 2559–2564. [CrossRef]
7. Wu, S.; He, M.; Yang, M.; Zhang, B.; Wang, F.; Li, Q. Near-Infrared Spectroscopy Study of Serpentine Minerals and Assignment of the OH Group. *Crystals* **2021**, *11*, 1130. [CrossRef]
8. Yariv, S. Infrared Evidence for the Occurrence of SiO Groups with Double-Bond Character in Antigorite, Sepiolite and Palygorskite. *Clay Miner.* **1986**, *21*, 925–935. [CrossRef]
9. Li, J. Research on Serpentine Jade from Ji'an City, Jilin Province. Master's Thesis, Jilin University, Changchun, China, April 2012.
10. Baatar, A.; Kim, W.S. Mineralogical Characteristics of Serpentine Jade and Thulite Gemminerals from Booyo Area, South Korea. In Proceedings of the European Geosciences Union General Assembly 2009, Vienna, Austria, 19–24 April 2009; p. 573.
11. Qin, H.; Liu, R. Mineral Composition and Genetic Analysis of Ji'an Serpentine Jade, Tonghua, Jinlin Province. *Acta Petrol. Mineral.* **2016**, *35*, 344–348.
12. Colman, S.M.; Pierce, K.L. Weathering Rinds on Andesitic and Basaltic Stones as a Quaternary Age Indicator, Western United States. *Geol. Surv. Prof. Pap.* **1981**. [CrossRef]
13. Dixon, J.C.; Thorn, C.E.; Darmody, R.G.; Campbell, S.W. Weathering Rinds and Rock Coatings from an Arctic Alpine Environment, Northern Scandinavia. *Geol. Soc. Am. Bull.* **2002**, *114*, 226–238. [CrossRef]
14. Grapes, R.H.; Yun, S.-T. Geochemistry of a New Zealand Nephrite Weathering Rind. *N. Z. J. Geol. Geophys.* **2010**, *53*, 413–426. [CrossRef]
15. Oguchi, C.T. Formation of Weathering Rinds on Andesite. *Earth Surf. Process. Landf.* **2001**, *26*, 847–858. [CrossRef]
16. Zhang, Z. Study on the Minerals Composition and Structural Characteristics of Weathering Crust of Primary Nephrite in Russia. Master's Thesis, China University of Geosciences (Beijing), Beijing, China, May 2019.
17. Colman, S.M. Rock-Weathering Rates as Functions of Time. *Quat. Res.* **1981**, *15*, 250–264. [CrossRef]
18. Oguchi, C.T. A Porosity-Related Diffusion Model of Weathering-Rind Development. *CATENA* **2004**, *58*, 65–75. [CrossRef]
19. Oguchi, C.T.; Matsukura, Y. Effect of Porosity on the Increase in Weathering-Rind Thicknesses of Andesite Gravel. *Eng. Geol.* **2000**, *55*, 77–89. [CrossRef]
20. Tang, C.; Shi, B.; Wang, B. Factors Affecting Analysis of Soil Microstructure Using SEM. *Chin. J. Geotech. Eng.* **2008**, *30*, 560–565.
21. Xiong, C.; Tang, H.; Liu, B.; Zhang, J. Using SEM Photos to the Pore Structural Parameters of Soil Samples. *Earth Sci.-J. Univ. Geosci.* **2007**, *32*, 415–419.
22. Xu, R.; Deng, Y.; Xu, B.; Lai, J.; Zhan, X.; Xu, L.; Lu, J. Quantitative Analysis of Soft Clay Three-dimensional Porosity Based on SEM Image Information. *J. Earth Sci. Environ.* **2015**, *37*, 104–110.
23. Liu, L. Study on Origin, Factors and Grading of the Color of Turquoise from China. Master's Thesis, China University of Geosciences, Wuhan, China, May 2018.
24. Chen, S.; Zhu, Y.; Wang, H.; Liu, H.; Wei, W.; Fang, J. Structure Characteristics and Accumulation Significance of Nanopores in Longmaxi Shale Gas Reservoir in the Southern Sichuan Basin. *J. China Coal Soc.* **2012**, *37*, 438–444. [CrossRef]
25. Li, Z.; Shen, X.; Qi, Z.; Hu, R. Comparations Between Mercury Intrusion and Gas Adsorption for Pore Structure Characteristics of Shale. *J. Eng. Geol.* **2017**, *25*, 1405–1413. [CrossRef]
26. Liu, P.; Guo, H.; Shen, R.; Li, H.; Ren, H.; Zhang, C. Study of the Structure of Shale Based on Gas Adsorption Method and Mercury Intrusion method. *Mech. Eng.* **2018**, *40*, 514–519.
27. Yang, F.; Ning, Z.; Hu, C.; Wang, B.; Peng, K.; Liu, H. Characterization of Microscopic Pore Structures in Shale Reservoirs. *Acta Pet. Sin.* **2013**, *34*, 301–311. [CrossRef]
28. Colman, S. *Chemical Weathering of Basalts and Andesites; Evidence from Weathering Rinds*; U.S. Government Publishing Office: Washington, DC, USA, 1982.
29. Etienne, S. The Role of Biological Weathering in Periglacial Areas: A Study of Weathering Rinds in South Iceland. *Geomorphology* **2002**, *47*, 75–86. [CrossRef]
30. Etienne, S.; Dupont, J. Fungal Weathering of Basaltic Rocks in a Cold Oceanic Environment (Iceland): Comparison between Experimental and Field Observations. *Earth Surf. Process. Landf.* **2002**, *27*, 737–748. [CrossRef]
31. Butler, D.R. Rock Coatings.: R. Dorn. Elsevier, Amsterdam, 1998. Developments in Earth Surface Processes 6, Hardbound, Xii and 429 Pages. Price US$207.00, ISBN 0-444-82919-9. *Geomorphology* **2000**, *33*, 123–124. [CrossRef]
32. Adsorption of Gases in Multimolecular Layers. *J. Am. Chem. Soc.* **1938**, *60*, 309–319. [CrossRef]
33. Barrett, E.P.; Joyner, L.G.; Halenda, P.P. The Determination of Pore Volume and Area Distributions in Porous Substances. I. Computations from Nitrogen Isotherms. *J. Am. Chem. Soc.* **1951**, *73*, 373–380. [CrossRef]
34. Sing, K.S.W. Reporting Physisorption Data for Gas/Solid Systems with Special Reference to the Determination of Surface Area and Porosity (Recommendations 1984). *Pure Appl. Chem.* **1985**, *57*, 603–619. [CrossRef]

35. Brunauer, S.; Deming, L.S.; Deming, W.E.; Teller, E. On a Theory of the van Der Waals Adsorption of Gases. *J. Am. Chem. Soc.* **1940**, *62*, 1723–1732. [CrossRef]
36. Sun, W.; McDonough, W. Chemical and Isotopic Systematics of Oceanic Basalts: Implications for Mantle Composition and Processes. *Geol. Soc. Lond. Spec. Publ.* **1989**, *42*, 313–345. [CrossRef]
37. Zhang, Y.; Jiang, Z.; Li, S.; Wang, Y.; Yu, L. The Process of Oceanic Peridotite Serpentinization: From Seafloor Hydration to Subduction Dehydration. *Acta Petrol. Sin.* **2022**, *38*, 1063–1080. [CrossRef]
38. Tang, Y.; Jia, J.; Xie, X. Environment Significance of Clay Minerals. *Earth Sci. Front.* **2002**, *30*, 337–344.
39. Biscaye, P.E. Mineralogy and Sedimentation of Recent Deep-Sea Clay in the Atlantic Ocean and Adjacent Seas and Oceans. *Geol. Soc. Am. Bull.* **1965**, *76*, 803–832. [CrossRef]
40. Huang, J. Study on Spectroscopy and Color-causing Mechanism of Anlu Jade. *Volcanol. Miner. Resour.* **1992**, *13*, 71–78.
41. Wang, Y.; Gan, F. Coloration Mechanism and Chromaticity of Xiuyan Jade of China. *Spectrosc. Spectr. Anal.* **2012**, *32*, 2305–2310.
42. Walter, L.M.; Huston, T.J.; Stueber, A.M. Br-Cl-Na systematics in Illinois basin fluids: Constraints on fluid origin and evolution. *Geology* **1990**, *18*, 315–318. [CrossRef]
43. Yang, J.; Zhang, Y.; Qiu, Z.; Jia, D.; Zheng, X. Geochemistry and Petrogenesis of Greenstone Belt Type Serpentine Jade from Taishan, Shandongd. *Geotecton. Metallog.* **2021**, *45*, 1044–1059. [CrossRef]
44. Leeman, W. Petrogenesis of McKinney (Snake River) Olivine Tholeiite in Light of Rare-Earth Element and Cr/Ni Distributions. *Geol. Soc. Am. Bull.* **1976**, *87*, 1582–1586. [CrossRef]
45. Liu, Y. Metallogenic Regularity and Prospecing Indicator of the Jade Deposit in the Xiuyan Area, Liaoning Province. Master's Thesis, Jilin University, Changchun, China, November 2013.
46. Dong, J.; Wang, Y.; Gan, F.; Li, Q. Trace Element Analysis by PIYE and ICP-AES of Raw Material and Ancient Serpentine Artifacts from China. *Guang Pu Xue Yu Guang Pu Fen Xi Guang Pu* **2016**, *36*, 3780–3788.
47. Zhuo, S.; Liu, Y.; Wang, J.; Jia, H.; Fu, Z.; Chi, H.; Mei, S.; Guo, P. The Petrological and Geochemical Characteristics of the Serpentinized Marble in the Wusutu Region, Inner Mongolia, China. *Bull. Mineral. Ptrol. Geochem.* **2016**, *35*, 239–246+1. [CrossRef]
48. Taylor, S.R.; McLennan, S.M. *The Continental Crust: Its Composition and Evolution*; Blackwell Scientific Publications: Oxford, UK, 1985; 312p.
49. Jewell, P.W.; Stallard, R.F. Geochemistry and Paleoceanographic Setting of Central Nevada Bedded Barites. *J. Geol.* **1991**, *99*, 151–170. [CrossRef]